Investigation of diffusion and electromigration parameters for Cu–Sn intermetallic compounds in Pb-free solders using simulated annealing

Brook Chao *, Seung-Hyun Chae, Xuefeng Zhang, Kuan-Hsun Lu, Jay Im, P.S. Ho

Laboratory for Interconnect and Packaging, The University of Texas at Austin, TX 78712, USA

Abstract

An efficient numerical method was developed to extract the diffusion and electromigration parameters for multi-phase intermetallic compounds (IMC) formed as a result of material reactions between under bump metallization (UBM) and solder joints. This method was based on the simulated annealing (SA) method and applied to the growth of Cu–Sn IMC during thermal aging and under current stressing in Pb-free solder joints with Cu-UBM. At 150 °C, the diffusion coefficients of Cu were found to be $3.67 \times 10^{17}\,\mathrm{m^2\,s^{-1}}$ for Cu_3Sn and $7.04 \times 10^{16}\,\mathrm{m^2\,s^{-1}}$ for Cu_6Sn_5, while the diffusion coefficients of Sn were found to be $2.35 \times 10^{16}\,\mathrm{m^2\,s^{-1}}$ for Cu_3Sn and $6.49 \times 10^{16}\,\mathrm{m^2\,s^{-1}}$ for Cu_6Sn_5. The effective charges of Cu were found to be 26.5 for Cu_3Sn and 26.0 for Cu_6Sn_5, and for Sn, the effective charges were found to be 23.6 for Cu_3Sn and 36.0 for Cu_6Sn_5. The SA approach provided substantially superior efficiency and accuracy over the conventional grid heuristics and is particularly suitable for analyzing many-parameter, multi-phase intermetallic formation for solder systems where quantitative deduction for such parameters has seldom been reported.
© 2007 Acta Materialia Inc. Published by Elsevier Ltd. All rights reserved.

Keywords: Electromigration; Diffusion; Intermetallic compound; Simulated annealing; Inversion

1. Introduction

In recent years, flip-chip technology has been widely accepted for high-density packages since the inception of C4 (controlled collapse chip connection) technology by IBM in the 1950s. The demand for flip-chip packages has seen tremendous growth over the past decade in applications such as microprocessors, graphics processors, high-end chipsets, cellular telecommunications and portable electronics. The drive to go Pb-free has quickly built momentum in the electronic industry in view of the potential hazards posed by the usage of Pb and its compounds in the conventional solder bumping process. This has raised serious reliability concerns because of the simultaneous demand for higher current density with smaller bump size for the Pb-free solder materials.

The formation of intermetallic compounds (IMC) as a result of material reaction between the under bump metallization (UBM) and solder joint during thermal aging has been extensively studied [1]. Under electromigration (EM), the growth of IMC can be significantly enhanced by mass transport driven by the electron current [2,3] and the IMC growth is accompanied by Kirkendall void formation, which plays an important role in controlling the EM lifetime of solder joints in flip-chip packages [3,4]. Ding [3] and Chae [4] both reported accelerated solder lifetime tests using a high resolution Wheatstone bridge method. While this method provided the sensitivity and accuracy required to correlate the intermetallic growth to the EM lifetime statistics of the solders, the materials parameters of diffusivity and effective charge that control the mass transport and the growth rate of multi-component IMC have not

* Corresponding author. Tel.: +1 512 471 8990; fax: +1 512 471 8969.
E-mail address: brookchao@mail.utexas.edu (B. Chao).

been determined so far. Such parameters are essential for quantitative analysis of the kinetics for IMC growth and EM damage and for optimum design of UBM and Pb-free solders.

This paper reports a numerical optimization method for simultaneous extraction of diffusion and electromigration parameters from two parallel experiments, thermal aging and electromigration, performed at the same temperature. It will become clear that the diffusion and EM parameters define complex non-linear growth kinetics of multi-component IMC in solder alloys. For the case studied in this paper of the Sn–Ag solder reaction with Cu UBM, two IMC – Cu_3Sn and Cu_6Sn_5 – were formed. The kinetic analysis has to be applied not only to the growth of the two compounds, but also must be traced to the starting Cu/Sn–Ag diffusion couple. For each of the phases, there are four parameters – component diffusivities and EM effective charges for Cu and for Sn – so the problem can become quite complex and it may be difficult to extract pertinent parameters simultaneously. In this paper, the extraction of the parameters is based on a Monte Carlo simulation technique known as simulated annealing (SA) [5] fitting to the observed intermetallic thicknesses at a given time. This method was applied to the formation of IMC Cu_3Sn and Cu_6Sn_5 from Sn–Ag solder joints with a Cu-UBM. We successfully derived the parameters of the diffusion coefficients and effective charge numbers for Cu and Sn in the intermetallics Cu_3Sn and Cu_6Sn_5, which to our knowledge have not been reported in the literature. The validity of the analysis and the deduced values will be discussed.

2. Experiment

2.1. Aging experiment

An aging experiment reported by Siewert et al. [6] was adopted in this paper. In their experiment, Sn–3.5Ag solder was deposited onto the sample coupons by melting the solders at 50 °C above the melting temperature. The coupons were pre-plated with 45–50 μm Cu and the Cu surfaces were cleaned prior to solder deposition by rinsing with ethanol and then a water-based solution of ammonium hydroxide, trisodium phosphate and sodium tetraborate pentahydrate. The coupons were then thermally aged in an oven at 150 °C, purged with industrial-grade Ar gas to prevent oxidation during thermal aging. The intermetallic growth was determined by measuring the thickness of each phase in cross-sectional scanning electron microscope (SEM) images.

2.2. Electromigration experiment

In this paper, the EM experimental results of intermetallic growth used for parameter extraction were obtained in a study of Sn–3.5Ag lead-free solder bumps with a Cu-based UBM stack as shown in Fig. 1a and b [4]. The test struc-
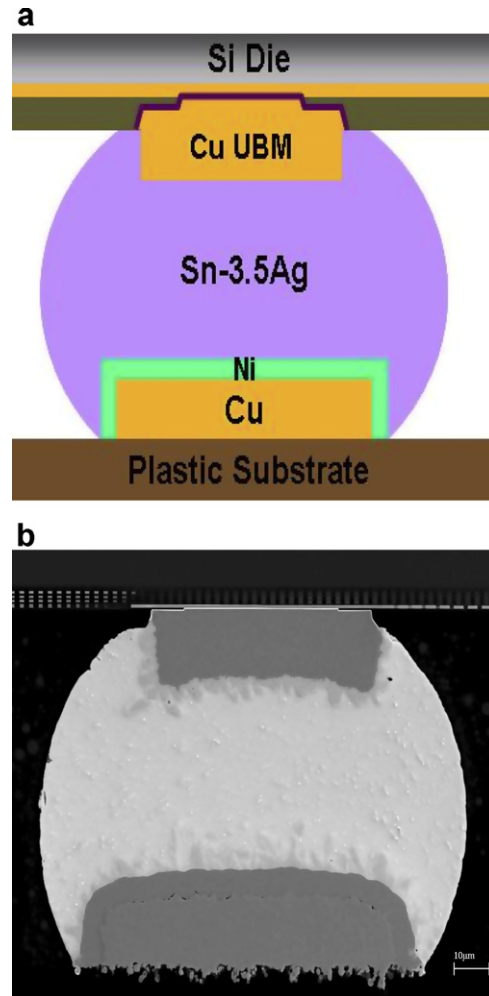

Fig. 1. (a) Schematic of a solder bump prior to current stressing and (b) cross-section image of a solder bump prior to current stressing.

tures were subjected to high current stressing ($\sim 5.16 \times 10^4$ and 4.12×10^4 A cm^{-2}) at an elevated temperature (~ 140 °C) for a prolonged period of time (>400 h) to observe enhancement effects on IMC growth kinetics and Kirkendall void formation. Current density was calculated by dividing the current by the area of the passivation opening. To facilitate minimization of the Joule heating effect that raises the solder temperature, all samples were attached to a Cu heat sink on the Si die side. Thermocouples were sandwiched between the Si dies and the heat sink to monitor the Si backside temperature. The oven temperature was carefully adjusted so that the Si backside temperatures of all samples were kept steadily at 140 °C. In order to account for the Joule heating effect and obtain the actual solder temperature, we measured the resistance changes as a function of temperature and applied current, and supplemented the experimental results with a finite element analysis (FEA) of the temperature distribution of the solder. Fig. 2a and b show the simulated temperature distribution of the solder joint under current stressing of 4.12×104 and 5.16×104 A cm^{-2} and the solder temperature was found
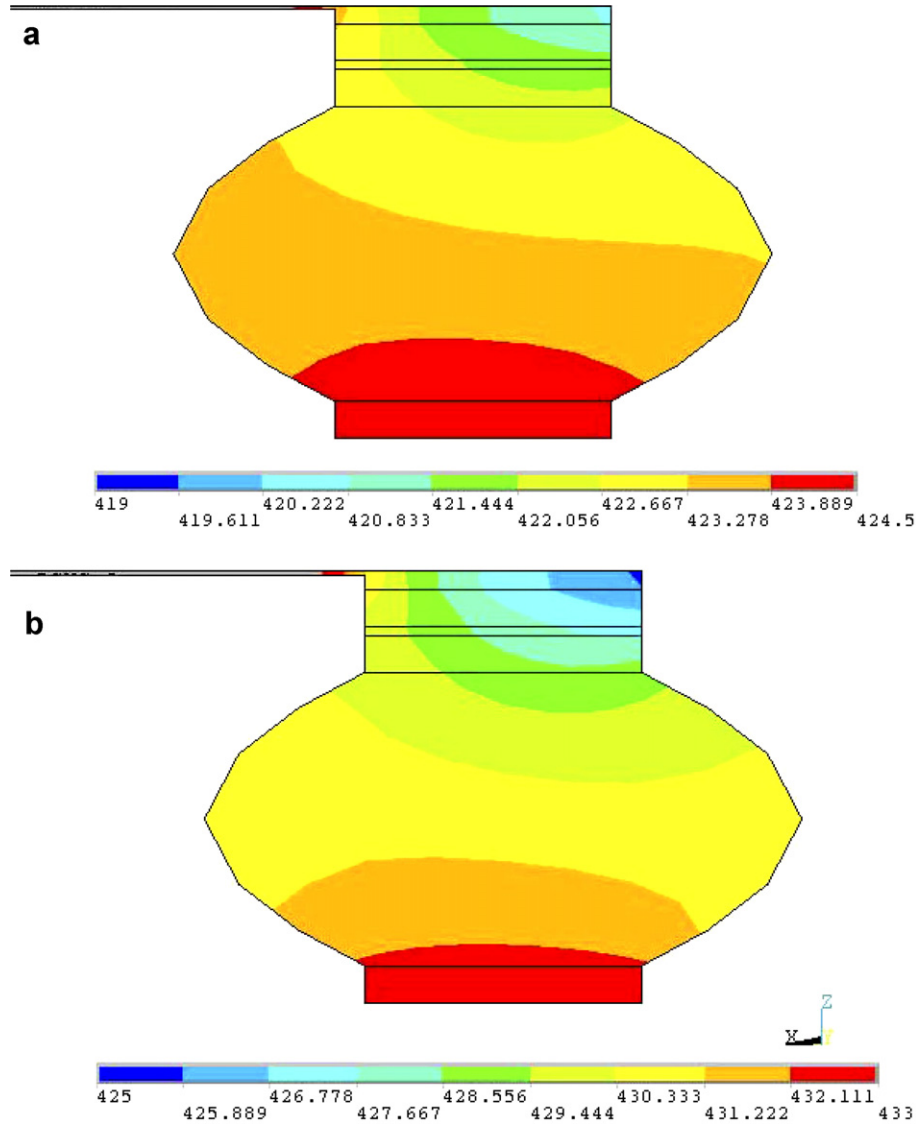
Fig. 2. Solder temperature distribution, in Kelvin: (a) 4.12×10^4 A cm^{-2} and (b) 5.16×10^4 A cm^{-2}.

to be around 10–15 °C above the measured Si backside temperature. The derivation of solder temperature was reported in a previous publication [4].

In the EM tests, electron current flowed from the under bump metallurgy to the top surface metallurgy (TSM). Cross-sectional SEM images were taken to observe the evolution of IMC phases as shown in Fig. 1b. Each phase was identified by energy-dispersive X-ray analysis (EDX) performed in the scanning electron microscope. Due to the non-planar nature of the Cu$_6$Sn$_5$ phase, the nominal thickness was calculated by dividing the cross-sectional area of the IMC by the initial width of the corresponding UBM.

3. Theory

3.1. Intermetallic growth kinetics

Chao et al. [7] showed that, for a diffusion couple with intermetallics, the migration of the interfaces due to the combined effect of thermal aging and EM can be expressed as the following equation:

$$v = \frac{\mathrm{d}x}{\mathrm{d}t} = v_{\text{Chem}} + v_{\text{EM}} = \frac{1}{C_{\alpha\beta} - C_{\beta\alpha}} \left\{ \left(\tilde{D}_\beta \frac{\partial C_\beta}{\partial x} - \tilde{D}_\alpha \frac{\partial C_\alpha}{\partial x} \right) \right.$$
$$\left. + j[C_{\beta\alpha}(C_0 - C_{\beta\alpha})\tilde{\phi}_\beta - C_{\alpha\beta}(C_0 - C_{\alpha\beta})\tilde{\phi}_\alpha] \right\} \quad (1)$$

As shown in Fig. 3, α and β represent the two adjacent phases separated by the interface of interest, $C_{\alpha\beta}$ and $C_{\beta\alpha}$ represent the compositions of the two phases at this interface and j denotes the current density applied to the sample. In Eq. (1), the second term in the bracket containing j comes from EM which gives a non-linear functional dependence on composition, in contrast to the first term which comes from thermal aging. The combination of these two terms leads to rather complex kinetics of compound growth depending on the aging and EM test conditions, as will be elaborated in the following.
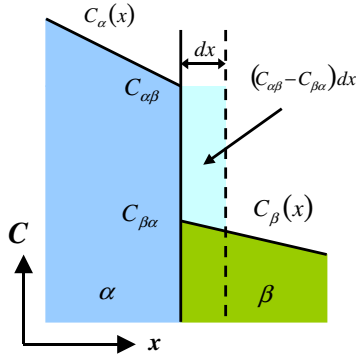
Fig. 3. Composition profile near an interface.

The two relevant parameters are defined as follows: the interdiffusion coefficient

$$\tilde{D} = X_{Cu}D_{Sn} + X_{Sn}D_{Cu} = D_{Cu} + (D_{Sn} - D_{Cu})\frac{C}{C_0} \qquad (2)$$

and the effective interdiffusion–electromigration coefficient,

$$\tilde{\phi} = D_{Sn}\phi_{Sn} - D_{Cu}\phi_{Cu} \qquad (3)$$

where $\phi = \frac{Z^*}{kT}e\rho$ is the electromigration factor, Z^* is the effective charge number, T is the temperature in Kelvin, e is the electron charge and ρ is the resistivity of the phase of interest.

According to Eq. (1), each compound phase grows or shrinks as a result of the migration of its interfacial boundaries and therefore the intermetallic thickness evolution can be obtained by numerically performing the following integration:

$$d = d_0 + \int_{t_0}^{t}(v_r - v_l)\,dt \qquad (4)$$

where v_l, v_r are the moving velocities of the left and right interfaces and d_0 is the initial IMC thickness.

3.2. Objective function

The objective function measures the misfit between the data and the corresponding modeling result. The optimal solution of the model parameters can be achieved by finding the minimum in the objective function. A least-squares approach is commonly used for its intimate relation with the Gaussian distribution, in which random errors are expected to occur. In this paper, the objective function is defined with respect to formation of IMC as:

$$S(m) = \frac{1}{N}\sum_{n}\sigma\left[\frac{d_n(m) - \bar{d}_n}{\bar{d}_0}\right]^2 \qquad (5)$$

where N is the total number of observables, n is the running index for the individual observable (IMC thickness), d_n is the theoretical value of the IMC thickness as derived from numerically integrating Eq. (4), $\bar{d}_0$ is the initial IMC thickness as measured from SEM images of intact solders, $\bar{d}_n$ is the IMC thickness at a given observation time as measured

from SEM images, m is the model parameter set (diffusion coefficients D and effective charge number Z^*) and σ is a weight parameter. It is worth noting that, as the model parameter set m is varied in a random fashion, each new m set would generate a new d_n set and therefore it is expressed as $d_n(m)$ in Eq. (5).

3.3. Simulated annealing

SA, proposed by Kirkpatrick et al. [5], is a Monte Carlo method that utilizes an analogy between the process of physical annealing and the mathematical solution of the global minimum of a function in which local minima may be present. The SA algorithm in this paper started with the identification of the model parameters to be extracted (D and Z^* of Cu and Sn in each phase) and the experimental observables (IMC thickness at given time). An objective function S was defined by Eq. (5) to be associated with multi-phase compound formation, so that the function could reach its global minimum when the optimized fit of the observables was achieved. The system was then subject to random walks over the entire model space in search of the optimal fit of the identified parameter set in a heuristic fashion. Numerical integrations based on Eq. (4) were performed dynamically for each attempted move to calculate the IMC thicknesses at the experimental observation time. The results were taken into the objective function and the moves were accepted or rejected based on the famous Metropolis criterion [8]:

$$P_{AB} = \min(1, e^{-(S_A - S_B)/\Theta}) \qquad (6)$$

where P_{AB} is the probability of acceptance of the transition from the model space A to the model space B and Θ is the nominal temperature.

To simulate the physical annealing process, the nominal temperature Θ was gradually decreased and it was adjusted so that the acceptance rates of the unfavorable moves reached approximately 50% at the onset and <10% at the end of the simulation. The rationale of the controlled cooling schedule is to prevent the system from being trapped at metastable states (local minima) so that the stable state (global minimum) will be invariably reached. A periodic boundary condition was applied to the entire model space to ensure its full exploration during the simulation. It is important to note that the diffusion coefficients and effective charge numbers should be modeled in different manners. The effective charge number Z^* should be modeled in a linear space because a possible range of 1–100 is more than enough to describe the solution space of Z^*. Nevertheless, the solution spaces of diffusion coefficients span over many orders of magnitude, therefore they should be modeled in a logarithmic space so as to have equal resolution within each order. Finally, the diffusivity and the effective charge parameters obtained in the simulation were used to calculate the compound growth rates and checked against experimentally observed results.

4. Results and discussion

Because of the difficulty in deriving the analytical solution for a multi-phase moving boundary problem, it is common in thermal aging analysis to take on the following empirical form to express the temporal relation of phase growth by a diffusion-controlled mechanism.

$$\Delta x(t) = kt^{1/2} \tag{7}$$

where k is the growth constant.

Although this parabolic law usually fits the aging data fairly well, there are still a few shortcomings when further analysis is required. First, Chao et al. [7] showed that IMC growth kinetics followed a linear law under substantial current stressing and the parabolic law was only valid for thermal aging or when current density was relatively insignificant. Second, the relation in Eq. (7) is empirical and it does not shed light on the mass transport taking place during IMC growth. Additionally, in quantitative analyses, the relation of the growth constant with temperature and current density is critical. Although the growth constant can be justified to be related with temperature through an Arrhenius relation, its relation with current density was never clear. However, based on the kinetic equations – Eqs. (1) and (4) – governing compound growth, quantitative analyses can be conducted using the component diffusion coefficients and effective charge number extracted to check against experimentally observed results without the restriction of uncertain empirical relations.

We previously reported a numerical analysis of EM-enhanced IMC growth based on a finite-difference model of a multiphase moving boundary diffusion problem [7]. This model does not rely on empirical relations, but was entirely based on physical driving forces, taking into account the diffusive fluxes resulting from both interdiffusion and EM. Knowledge of the diffusion coefficients (D)

and the effective charge numbers (Z^*) is essential to the success of the modeling. However, most of these parameters are not readily available in the literature. We therefore propose simultaneous extraction of the diffusion and EM parameters based on SA analyses of the experimental IMC growth data. The intermetallic growth under current stressing is controlled by the balance of the diffusive fluxes due to interdiffusion and electromigration [7,9,10]. As a consequence, experimental data of intermetallic growth should contain the parametric information and it is in theory viable to deduce the parameters from the intermetallic growth data.

4.1. Diffusion coefficients

Table 1 lists the diffusion coefficients of interest and their temperature relation as reported in the literature [11–20]. Diffusion coefficients can be expressed as a function of temperature in the following Arrhenius relationship:

$$D = D_0 \exp \left(\frac{Q}{RT} \right)$$

where D is the diffusion coefficient, D_0 is the intrinsic diffusivity of the material, Q is the activation energy for diffusion, R is the gas constant and T is the temperature in Kelvin.

The coefficients of self-diffusion in pure Cu and pure Sn phases are readily available in ASM and diffusion handbooks [11–13]. Sn has been identified as having a tetragonal crystal structure [21] and its anisotropic diffusion coefficients have been reported [13]. Since the interdiffusion model in this paper is unidimensional, this anisotropy was neglected and only one diffusion coefficient was used for Sn self-diffusion [11]. Dyson et al. [14] reported that mobility of Cu in the pure Sn phase was extremely rapid and anisotropic due to its fast diffusion by an interstitial

Table 1
Diffusion coefficients in literature

Type of diffusion	D_0 (m²/s)	Q (kJ/mol)	D (25 °C)	D (150 °C)	Condition	Reference
$D_{\text{Cu in (Cu)}}$	3.4×10^{-5}	195.6	2.29×10^{-39}	2.71×10^{-29}		[11]
	$6.0–7.8 \times 10^{-5}$	211.4–213.1	9.11×10^{-42}	5.42×10^{-31}		[12]
$D_{\text{Sn in (Sn)}}$	1.2×10^{-9}	43.89	2.58×10^{-17}	4.70×10^{-15}		[11]
	7.70×10^{-4}	107.1	1.50×10^{-22}	4.92×10^{-17}	∥c	[13]
	1.07×10^{-3}	105	4.85×10^{-22}	1.24×10^{-16}	⊥ c	[13]
$D_{\text{Cu in (Sn)}}$	2.4×10^{-7}	33.02	4.09×10^{-13}	2.05×10^{-11}	⊥c	[14]
			$\sim 2 \times 10^{-10}$		∥c	[14]
$D_{\text{Sn in (Cu)}}$	2.95×10^{-5}	177.0	3.53×10^{-36}	4.61×10^{-27}		[15]
	4.1×10^{-7}	129.8	7.97×10^{-30}	4.18×10^{-23}		[12]
$\tilde{D}_{\text{Cu}_3\text{Sn}}$	5.48×10^{-9}	61.86	8.54×10^{-20}	1.31×10^{-16}		[16]
	1.43×10^{-8}	70.6	6.63×10^{-21}	2.87×10^{-17}		[17]
	3.2×10^{-6}	83.91	7.01×10^{-21}	1.47×10^{-16}		[18]
	5.3×10^{-8}	66.1	1.50×10^{-19}	3.81×10^{-16}	Thin film	[19]
	8.08×10^{-7}	81.6	4.48×10^{-21}	7.15×10^{-17}	Single crystal	[19]
$\tilde{D}_{\text{Cu}_6\text{Sn}_5}$	1.84×10^{-9}	53.92	6.99×10^{-19}	4.19×10^{-16}		[16]
	1.55×10^{-8}	64.8	7.40×10^{-20}	1.61×10^{-16}		[17]
			$> 10^{-21}$		Thin film (no Cu₃Sn)	[20]

mechanism. They reported Cu diffusion parallel to the *c* direction to be ~500 times faster than perpendicular to it. However, we neglected this anisotropy of diffusion behavior in the Sn lattice. This simplification can be justified by the SEM images of IMC growth subject to substantial current stressing, as shown in Fig. 4. These SEM images did not show an enhanced growth along certain grain orientation. Instead, they showed strong correlation between the enhanced growth direction and the electron path through the solder. We, therefore, concluded that the anisotropy of Cu interstitial diffusion in the Sn lattice is relatively insignificant as compared with the rapid enhancement of phase growth by current stressing. The formation of Kirkendall voids at the IMC/Sn interface usually accompanies IMC growth in the solid state. Their effects have been extensively studied [3,4,7] and are not within the scope of this paper.

The diffusion coefficients of Cu and Sn atoms in the IMC are not widely documented. However, the interdiffusion coefficients of the Cu–Sn intermetallics have been reported by a number of research groups. Both Mei et al. [16] and Onishi et al. [17] deduced the interdiffusion coefficients by conducting an annealing experiment and fitting the analytical model to the experimental data. Although the intrinsic diffusivities and activation energies they deduced were different between the two groups, their results were reasonably consistent with each other in the values of the interdiffusion coefficients at the temperature of interest. Dreyer et al. [18] used differential scanning calorimetry to investigate the energetics and kinetics of interdiffusion of solder/metal diffusion couples and the interdiffusion coefficient of Cu_3Sn was alternatively derived.

4.2. Effective charge number

The electromigration driving force is measured by a dimensionless parameter, the effective charge number Z^*. Nowick and Burton [22] derived this driving force, which
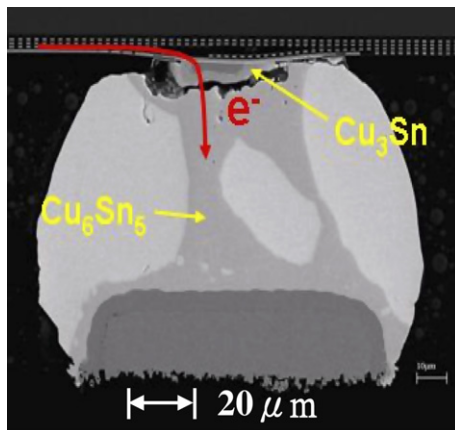
is comprised of the electrostatic and the electron wind contributions:

$$F_{\text{eff}} \equiv |e|Z * E = |e|(Z^{\text{e}} + Z^{\text{w}})E \qquad (8)$$

The electrostatic charge number Z^{e} represents the direct electrostatic force on the moving ion and hence its value is expected to be the nominal valence of the ion. The electron wind charge number Z^{w} accounts for the electron wind force which is generally the dominant contribution.

Self-electromigration has been reported for both Cu and Sn and their effective charge numbers have been determined [23–26]. However, the effective charge numbers of Cu and Sn as dilute solutes in each other have not been reported. Hsieh and Huntington [27] reported the effective charge number for Cu as dilute solute in pure Pb. The value fell in the range of 0.6–3.25. The electron wind charge numbers Z^{w} of Cu in Pb and in Sn are expected to be similar because Pb and Sn are both quadrivalent metals in group IV with similar electronic configurations and Cu atoms diffuse interstitially in both host metals. The effect on Z^{w} of ions taking on interstitial sites or substitutional sites was reviewed by Nowick and Burton [22]. Therefore, the effective charge number of Cu in pure Pb is herein taken to be the same as that in pure Sn, with reservation. Table 2 lists the literature-reported values of the effective charge numbers of interest [23–25,27,28].

4.3. Extracted parameters and their validity

Table 3 shows the derived model parameters in the intermetallics Cu_3Sn and Cu_6Sn_5, along with the values of those available in the literature. Since the diffusion coefficients of the individual species in the IMCs have never been reported, there are no literature values available for direct comparison. However, Mei et al. [16], Onishi et al. [17] and Dreyer et al. [18] reported the interdiffusion coefficients of these intermetallics. The diffusion coefficients are related to the interdiffusion coefficients through Eq. (2) and the interdiffusion coefficients calculated from the derived diffusion coefficients are consistent with the results given in Refs. [16–18], as shown in the table.

In addition, the diffusivities of Cu and Sn in the intermetallics were found to be close to each other within one order of magnitude. It has been argued that diffusion in highly ordered IMC occurs via more complex mechanisms because the simple nearest-neighbor jump of a vacancy will inevitably lead to disordering of the atomic structure. The concept of correlated nearest-neighbor vacancy jumping

Fig. 4. SEM image of a solder joint subject to prolonged current stressing.

Table 2
Effective charge numbers in literature

Species	Phase	Z^* Ref	Reference
Cu	Cu	2–7	[23–25]
	Sn	0.6–3.25 (Pb)	[27]
Sn	Cu	–	
	Sn	18	[28]

Table 3
Diffusion coefficients and effective charge number derived by solving the inverse problem of intermetallic growth rate at 150 °C

Phase	Diffusant	Z^*	D_{150} (m²/s)	Interdiffusion coefficient (m²/s)	Interdiffusion coefficient literature (m²/s)
Cu₃Sn	Cu	26.5	3.67×10^{-17}	1.87×10^{-16}	2.87×10^{-17} [17] $\sim 3.81 \times 10^{-16}$ [19]
	Sn	23.6	2.35×10^{-16}		
Cu₆Sn₅	Cu	26.0	7.04×10^{-16}	6.74×10^{-16}	1.61×10^{-16} [17] $\sim 4.19 \times 10^{-16}$ [15]
	Sn	36.0	6.49×10^{-16}		

that maintains the atomic ordering was first proposed for the B2 atomic structure by Elcock and McCombie [29] and Huntington et al. [30] and was named the six-jump cycle (6JC) or Huntington–McCombie–Elcock (HME) mechanism. The immediate result of the correlated jump mechanisms is the strong coupling between the component diffusivities of the intermetallics. Bakker [31] indicated that the 6JC mechanism imposed limits on the ratio of the component diffusivities as follows:

$$0.5 < D_A^*/D_B^* < 2 \tag{9}$$

where D_A^* and D_B^* are the component tracer diffusion coefficients. Due to experimental errors which inevitably occur, the diffusion coefficients derived in this paper were not sufficiently definite to substantiate this relation. However, the ratios of the component diffusion coefficients (D_{Cu}^*/D_{Sn}^*) derived in this paper were 0.16 and 1.08 for Cu₃Sn and Cu₆Sn₅, respectively, and they were not far off, if not within the limits. Special attention needs be paid to the ratio for Cu₆Sn₅. Although the Cu₆Sn₅ structure is of B8-type, its composition range is ∼0.54–0.55, which is close to the ideal composition, 0.5, of a B2-type structure. One would therefore expect the component diffusion coefficients of Cu₆Sn₅ to follow a relation close to Eq. (9) and the ratio obtained for Cu₆Sn₅ in this paper appears to be reasonable in this respect.

Although the effective charge number Z^* measures the strength of the EM driving force, the induced diffusive flux is still restrained by the diffusivity of the species in the phase of interest. Therefore, drift velocity is controlled by the product of diffusivity and effective charge number, DZ^*, rather than Z^* alone. In order to decouple Z^* from D, knowledge of D is essential to the quantitative analysis. The decoupling of D and Z^* can be challenging because the model space of the diffusion coefficients spans several orders of magnitude, while the model space of 1–100 is considered sufficient for effective charge number. Therefore, the simultaneous fitting of thermal aging data are required to anchor the values of the diffusion coefficients in the heuristic search for the optimal values of the effective charge number. The effective charges of Cu were found to be 26.5 for Cu₃Sn and 26.0 for Cu₆Sn₅, and for Sn the effective charges were found to be 23.6 for Cu₃Sn and 36.0 for Cu₆Sn₅.

4.4. IMC growth: mechanisms, morphologies and kinetics

After deriving the parameters, they were subsequently taken into the previously reported IMC kinetic simulation [7]. Fig. 5 shows the IMC growth kinetics for thermal aging. Fig. 5a was plotted against time and Fig. 5b was plotted against square root of time. The growth kinetics of both Cu₃Sn and Cu₆Sn₅ clearly followed parabolic laws, indicating the IMC growth to occur in a diffusion-controlled mechanism. Fig. 6 shows the EM-enhanced IMC growth kinetics under two current stressing conditions (4.12×10^4 and 5.16×10^4 A cm⁻²). The IMC growth clearly changed from parabolic kinetics to linear kinetics when substantial current density was applied. It was also noticeable that the simulated trend matched well with experimental observations for both thermal aging (Fig. 5)
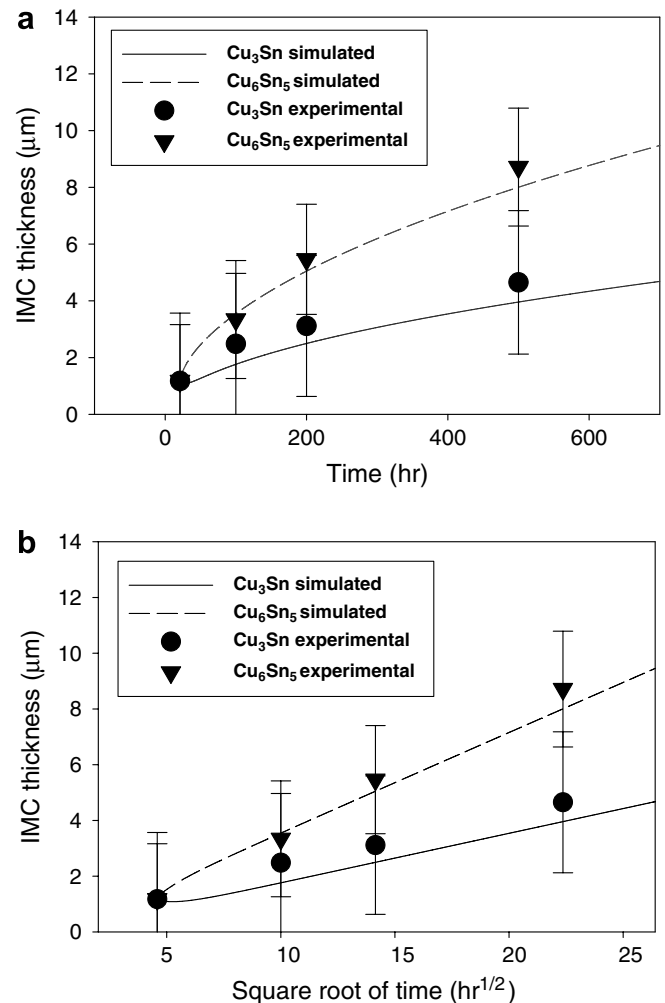

Fig. 5. IMC growth for thermal aging (a) plotted against time and (b) plotted against square root of time.
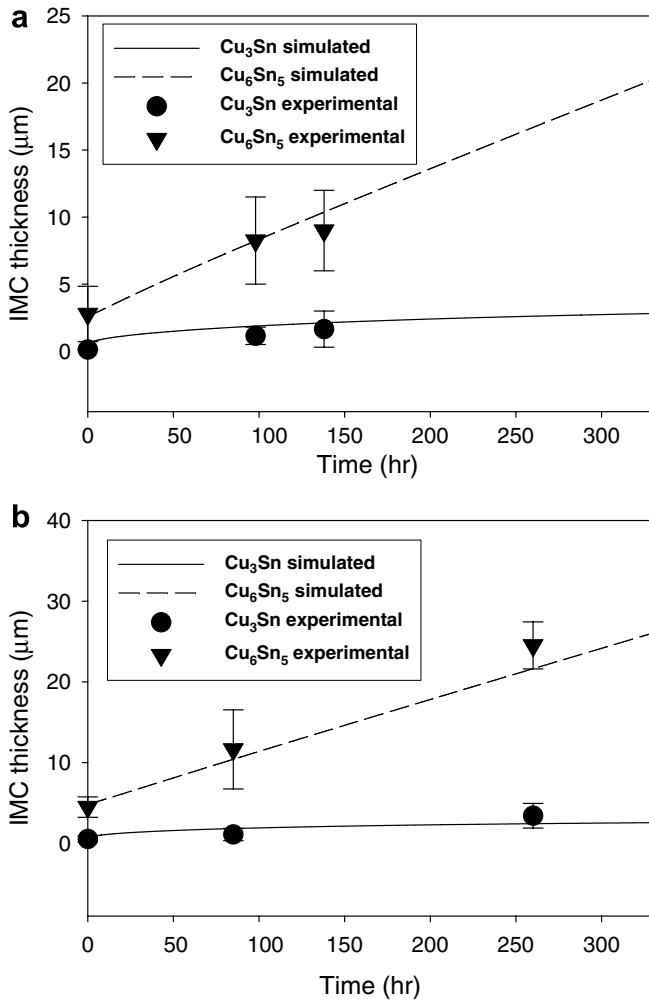
Fig. 6. Electromigration enhanced IMC growth under (a) 4.12×10^4 A cm^{-2} and (b) 5.16×10^4 A cm^{-2}.

and EM under various current densities (Fig. 6). Detailed discussion regarding the IMC kinetic analysis and the associated Kirkendall void formation can be found in a previous publication [7] and therefore is not covered in this paper.

The objective of this paper was to establish an efficient methodology to derive the parameters that directly correlate the diffusion and EM driving forces to the IMC growth kinetics. Due to the non-linear and complex nature of the system, the use of a one-dimensional model is critical because it greatly simplifies the problem and renders a practical computational cost. However, the disadvantage of a one-dimensional diffusion model is its inadequacy in addressing non-planar morphologies. In order to understand the non-planarity of IMC, it is important to distinguish the reflow reaction, one that occurs at solid–liquid interfaces, and the subsequent aging and EM reactions, that occur at solid–solid interfaces.

For the reflow reaction, Kim et al. [32] indicated that the size of Cu$_6$Sn$_5$ scallops approximately follows $t^{1/3}$ dependence growth kinetics, t being the reflow time, and the scal-

lops form by Ostwald ripening reactions. Görlich et al. [33] indicated that the wetting angle between adjacent scallops is an equilibrium feature at the reflow temperature and is related to the surface tension balance between the molten solder/Cu$_6$Sn$_5$ interface and the grain boundary. From these two studies, it was obvious that, during reflow reactions, the IMC morphology and its growth kinetics are different from the phase growth in the solid state.

For solid-state aging, Tu et al. [34] found that, for eutectic SnPb solder, the Cu$_6$Sn$_5$ morphology gradually changed from scallop type, as formed in reflow, to layer type. They also indicated that the solid-state aging kinetics follow a parabolic law, suggesting a diffusion-controlled mechanism. In our previous paper [7], it was confirmed that the parabolic kinetics can be explained by the flux-driven IMC growth model. In EM, however, we have shown that Cu$_6$Sn$_5$ growth can be significantly enhanced by current along the electron path [4] and that the growth kinetics follows a linear law, which suggests a reaction-controlled mechanism [7].

The comparisons between the Cu/Sn reactions during reflow, aging and EM are summarized in Table 4. Although the equilibrium IMC morphologies of these reactions are different, their kinetic behaviors can be explained by flux-driven approaches. Gusak and Tu [35] devised a flux-driven ripening theory to explain the growth kinetics and size distribution of Cu$_6$Sn$_5$ scallops during solder reflow reactions. We presented in previous work [7] and in this paper a kinetic model that takes into account both diffusion- and EM-induced flux. This model can therefore explain the kinetic behaviors of solid-state aging and EM based on the current density given.

It is worth noting the effect of the reaction history on the analysis of the solder/UBM structure. As indicated by Tu et al. [34], the kinetics of reflow reactions can be four orders of magnitude faster than solid-state aging. Therefore, despite the tendency of IMC to show layer-type morphology, the Cu$_6$Sn$_5$ phase can still exist in scallop shapes even after a prolonged solid-state aging. However, high current stressing can substantially increase the solid-state kinetics and completely alter the morphology within the same reaction time [4].

4.5. Simulated annealing vs. grid heuristics

The most common and straightforward method to extract parameters from experimental data are to conduct a grid search for the minimum of the objective function. However, for a many-parameter extraction, grid heuristics exhibits a prohibitive computational cost and suffers poor resolution and accuracy. Fig. 7 shows the contour plot of a hypothetical two-parameter system and the solution space is meshed with a grid resolution of 1/10 of the span. It is apparent that the solution (global minimum) is situated at $(X, Y) = (7.5, 2.5)$; however, due to the coarsely meshed grid network, an erroneous result of $(X, Y) = (5, 7)$ may be given. It is worth emphasizing that very fine

Table 4
Reactions at the solder/IMC interface

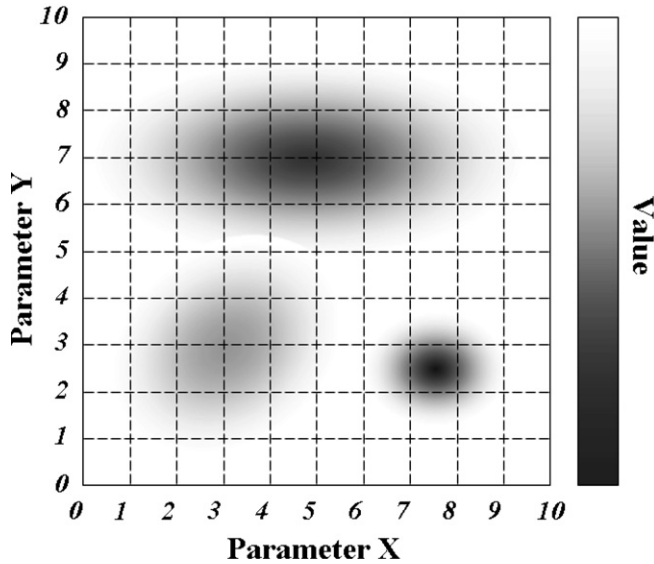| Reactions	Critical interface	IMC morphology		Mechanism	Kinetics	Reference
		Cu_3Sn	Cu_6Sn_5			
Reflow	Solid/liquid	Layer	Scallop	Ostwald ripening	$t^{1/3}$	[32]
Aging	Solid/solid	Layer	Layer	Diffusion controlled	$t^{1/2}$	[35,7]
EM	Solid/solid	Layer	Electron path	Reaction controlled	t	[4,7]

Fig. 7. Contour plot of a hypothetical two parameter system with a grid resolution of 1/10 of the span of the individual parameter to be extracted (the functional values are represented by grayscale as shown in the grayscale bar).

meshing is impractical for a many-parameter system because the number of grid nodes to be included in the calculation increases exponentially with the number of parameters.

Fig. 8 shows the moving average plot of three independent SA simulations to which identical conditions were applied except that the total numbers of Monte Carlo steps
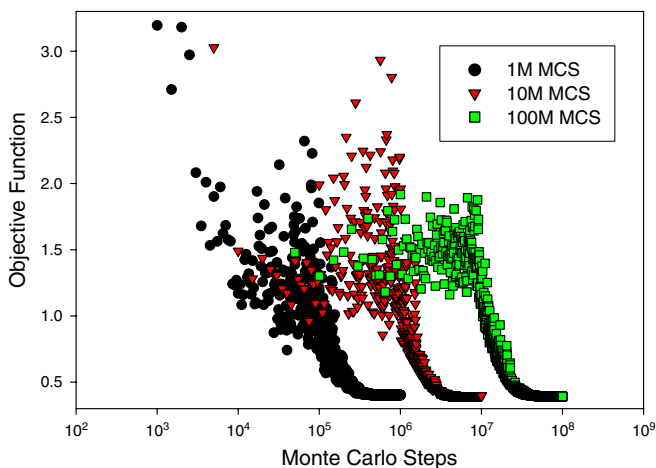
taken were 1, 10 and 100 million, respectively. There were 16 parameters including D and Z^* of Cu and Sn in all four phases. It was apparent that all three simulations reached the same eventual minimum. In a regular PC, the simulations took roughly 0.5, 5 and 50 min. However, if a grid heuristic technique was to be used with a 1/10 resolution, the number of steps required for this grid search would be 11^{16} and the expected simulation time escalates to 1600 days! SA is substantially more efficient and more accurate than grid heuristics for the following reasons. First, grid heuristics treats the entire solution space equally and goes through all grid nodes over the space, whereas SA only explores the valleys (metastable or stable states) and therefore is able to find the solution more efficiently. Moreover, the accuracy of grid heuristics is restricted by the grid resolution of the meshing, while SA is free of this limitation by taking variable step size random walks. Therefore, SA easily outperforms the grid search method in terms of efficiency and accuracy for a many-parameter extraction problem.

As a last remark, the minimization of the predetermined objective function does not guarantee the appropriate solution of a parameter extraction problem. Judgement based on a priori information must also be exercised to select the justifiable results. A priori information can also be included into the objective function to help anchor certain model parameters and stabilize the solution. However, in our first attempt at this problem, we avoided techniques of this kind and simply let nature take its course.

5. Conclusion

A new method of simultaneous extraction of diffusion and EM parameters of an intermetallic system was proposed based on SA inversion of IMC growth during thermal aging and under EM. The parameters for the application of a Pb-free solder with Cu-UBM and their associated IMCs were derived according to this method. The component diffusion coefficients of the IMC were justified by their corresponding interdiffusion coefficients and the ratios of the component diffusivities. The kinetic analysis for thermal aging and EM based on the derived parameters showed satisfactory fit with the experiments.

References

[1] Yeh ECC, Choi WJ, Tu KN, Elenius P, Balkan H. Appl Phys Lett 2002;80:580.

Fig. 8. Optimization of the objective function.

[2] Zeng K, Stierman R, Chiu TC, Edwards D, Ano K, Tu KN. J Appl Phys 2005;97:024508.

[3] Ding M, Wang G, Chao B, Ho PS, Su P, Uehling T. J Appl Phys 2006;99:094906.

[4] Chae SH, Zhang X, Lu KH, Chao HL, Ho PS, Ding M, et al. J Mater Sci: Mater Electr 2007;18:247.

[5] Kirkpatrick S, Gelatt CD, Vecchi MP. Science 1983;220:671.

[6] Siewert TA, Madeni JC, Liu S. In: Proceedings of APEX conference on electronics manufacturing; 2003.

[7] Chao B, Chae SH, Zhang X, Lu KH, Ding M, Im J, et al. J Appl Phys 2006;100:084909.

[8] Metropolis N, Rosenbluth A, Rosenbluth M, Teller A, Teller E. J Chem Phys 1953;21:1087.

[9] Gurov KP, Gusak AM. Phys Met Metallogr 1981;52(4):75.

[10] Gan H, Tu KN. J Appl Phys 2005;97:063512.

[11] Seith W, Heumann T. Diffusion of metals: exchange reactions. Washington, DC: United States Atomic Energy Commission; 1962. Translated from a publication of Springer, Berlin. p. 65, 68.

[12] Davis JR, editor. ASM specialty handbook: copper and copper alloys. Materials Park (OH): ASM International; 2001. p. 235.

[13] Seitz F, Turnbull D, Ehrenreich H, Peterson NL. Solid state physics, 22. New York (NY): Academic Press; 1968.

[14] Dyson BF, Anthony TR, Turnbull D. J Appl Phys 1967;38:3408.

[15] Hoshino K, Iijima Y, Hirano KI. Trans Jpn Inst Met 1980;21:674.

[16] Mei Z, Sunwoo AJ, Morris Jr JW. Metall Trans A 1992;23A:857.

[17] Onishi M, Fujibuchi H. Trans Jpn Inst Met 1975;16(9):539.

[18] Dreyer KF, Neils WK, Chromik RR, Grosman D, Cotts EJ. Appl Phys Lett 1995;67(19):2795.

[19] Bader S, Gust W, Hieber H. Acta Metall Mater 1995;43(1):329.

[20] Tu KN. Acta Metall 1973;21:347.

[21] Deshpande VT, Sirdeshmukh DB. Acta Crystallogr 1961;14:355.

[22] Nowick AS, Burton JJ. In: Huntington HB, editor. Diffusion in solids: recent developments. New York: Academic Press; 1974. p. 303–52.

[23] Grone AR. J Phys Chem Solids 1961;20:88.

[24] Sullivan GA. J Phys Chem Solids 1967;28:347.

[25] Grimme D. Atomic transport in solids and liquids. Tübingen: Verlag der Zeitschrift für Naturforschung; 1971.

[26] Liu CY, Chen C, Tu KN. J Appl Phys 2000;88(10):5703.

[27] Hsieh MY, Huntington HB. J Phys Chem Solids 1978;39:867.

[28] Khosla A, Huntington HB. J Phys Chem Solids 1975;36:395.

[29] Elcock EW, McCombie CW. Phys Rev 1958;109:605.

[30] Huntington HB, Miller NC, Nerses V. Acta Metall 1961;9:749.

[31] Bakker H. Philos Mag A 1979;40(4):525.

[32] Kim HK, Liou HK, Tu KN. Appl Phys Lett 1995;66(18):2337.

[33] Görlich J, Schmitz G, Tu KN. Appl Phys Lett 2005;86:053106.

[34] Tu KN, Lee TY, Jang JW, Li L, Frear DR, Zeng K, et al. J Appl Phys 2001;89(9):4843.

[35] Gusak AM, Tu KN. Phys Rev B 2002;66:115403.